Available online at www.sciencedirect.com
ScienceDirect
Image and Vision Computing 26 (2008) 690–701
www.elsevier.com/locate/imavis

Analytic image unwarping by a systematic calibration method for omni-directional cameras with hyperbolic-shaped mirrors

Sheng-Wen Jeng [a,*], Wen-Hsiang Tsai [a,b,1]

[a] Department of Computer Science, National Chiao Tung University, 1001 Ta Hsueh Road, Hsinchu 300, Taiwan
[b] Department of Computer Science and Information Engineering, Asia University, Liufeng Road, Wufeng, Taichung 41354, Taiwan

Received 12 November 2004; received in revised form 3 August 2007; accepted 8 August 2007

Abstract

Unwarping an omni-directional image into a perspective-view one is easy for a single-viewpoint (SVP) designed catadioptric omni-directional camera. But misalignment between the components (such as the mirror and the lens) of this kind of camera creates multiple viewpoints and distorts the unwarped image if the SVP constraint is assumed. The SVP constraint is relaxed in this study and a systematic method is proposed to derive a set of new and general analytic equations for unwarping images taken from an omni-directional camera with a hyperbolic-shaped mirror (called a hypercatadioptric camera). The derivation is made possible by careful investigation on the system configuration and precise calibration of involved system parameters. As a verification of the correctness of the derived equations, some of the system parameters are adjusted to fit the SVP constraint, and unwarped images using the resulting simplified camera model are shown to be of no difference from those obtained by a method based on the SVP model. The generality of the proposed method so has extended the image-unwarping capability of the existing methods for the hypercatadioptric camera to tolerate lens/mirror assembly imprecision, which is difficult to overcome in most real applications. Some experimental results of image unwarping are also included to show the effectiveness of the proposed method.

Keywords: Omni-directional camera; Single-viewpoint (SVP) constraint; Image unwarping; Hyperbolic mirror; Hypercatadioptric camera; Camera calibration; Analytic solution

1. Introduction

It is well known in the computer vision field that enlarging the field of view (FOV) of a camera enhances the visual coverage, reduces the blind area, and saves the computation time, of the camera system, especially in applications like visual surveillance and vision-based robot or autonomous vehicle navigation.

There are many ways to design a camera system consisting of CCD sensors, lenses, and mirrors to increase the FOV of the system [1]. An extreme way is to expand the FOV to a full hemisphere by the use of a *catadioptric camera*, which is an integration of a CCD sensor chip, a convex reflection mirror, and a projection lens. A popular name for this kind of camera is *omni-directional camera*, or simply *omni-camera*, and that for an image taken by it is *omni-directional image*, or simply *omni-image*. The surface curve of the reflection mirror in such a kind of camera may be conical, spherical, parabolic, or hyperbolic, and the lens may be of the type of orthographic or perspective projection. To simplify the process for unwarping omni-images into perspective ones, it is usually desired to design an omni-camera in such a way that the *single-viewpoint* (SVP) constraint is satisfied [2].

Only some of the possible mirror/lens combinations can fit the SVP constraint, for examples, a combination of a parabolic mirror and an orthographic lens or that of a

* Corresponding author. Tel.: +886 6 3847167.
E-mail addresses: sunny@itri.org.tw (S.-W. Jeng), whtsai@cis.nctu.edu.tw (W.-H. Tsai).
[1] Tel.: +886 3 5728368.

0262-8856/$ - see front matter © 2007 Elsevier B.V. All rights reserved.
doi:10.1016/j.imavis.2007.08.005

hyperbolic mirror and a perspective lens [2]. However, because of the difficulty in the alignment of the mirror and the camera lens, many commercial products do not satisfy the SVP constraint. When this case occurs, the resulting locus of viewpoints will form a so-called *caustic curve* [3] and the corresponding image unwarping work becomes very complicated. On the other hand, when the parabolic mirror/orthographic lens combination is used, the resulting system is called a paracatadioptric camera [8]. Following this idea of naming the camera system, when the hyperbolic mirror/perspective lens combination is used, the resulting system is called a *hypercatadioptric camera* in this paper. In this study, we deal with the image-unwarping problem for a hypercatadioptric camera in a non-SVP system.

More specifically, we propose in this study a systematic method to calibrate the system parameters of a hypercatadioptric camera and derive accordingly a set of equations for accurate image unwarping. In the proposed camera calibration process, a calibration pattern of the shape of a thin ring is designed and attached at the border of the mirror as an aid. Next, mirror reflection laws as well as system geometry constraints are utilized to derive a set of mapping equations between a pixel in the image coordinate system and a point in the world space. The calibrated system parameters are used as known parameters in the derivation. The derived equations are then used to unwarp accurately an omni-image taken by a hypercatadioptric camera into a perspective-view image from any viewpoint.

Several contributions are made by the proposed method. The first is that the derived image-unwarping equations are *analytic*. This is achieved for the first time, and the computation involved in the image unwarping work will so become faster. Another contribution is that unwarping of omni-images taken by a hypercatadioptric camera into perspective-view images will not be confined to the SVP constraint. And this makes the applicability of the hypercatadioptric camera much wider to various computer vision problems. Finally, the generality of the proposed method for non-SVP cameras has extended the image-unwarping capability of the existing methods for the hypercatadioptric camera to tolerate lens/mirror assembly imprecision, which is difficult to overcome in most real applications.

The remainder of this paper is organized as follows. In Section 2, we review the basic concepts about SVP omni-cameras and some previous works for omni-camera calibration. The camera calibration process proposed in this study is described in Section 3. In Section 4, the corresponding analytic image-unwarping equations are derived. In Section 5, some experimental results using simulation data as well as real images are given. Finally, some conclusions are made in Section 6.

2. Review of previous works

For an SVP catadioptric camera, unwarping an omni-image into a perspective version is a process of *forward projection* from a point X_p on a certain perspective-view plane in the world space to an omni-image point X_i, which can be described by $X_i = h(X_p)$ with h being a *one-to-one* mapping function from the world space to the omni-image plane [4,5]. For example, for an SVP hypercatadioptric camera, the mapping relation between a point $X_p(x,y,z)$ in a world space and its projection point $X_i(u,v)$ in the image plane, as illustrated in Fig. 1, is as follows:

$$u = \frac{f(b^2-c^2)x}{(b^2+c^2)z - 2bc\sqrt{x^2+y^2+z^2}},$$
$$v = \frac{f(b^2-c^2)y}{(b^2+c^2)z - 2bc\sqrt{x^2+y^2+z^2}}, \quad (1)$$

where f is the focal length of the camera lens, and a, b, and c are the parameters of the hyperbolic curve of the mirror surface described as follows:

$$z = -c + b\sqrt{1+\frac{r^2}{a^2}}, \quad r^2 = x^2+y^2 \quad (2)$$

with $c = \sqrt{a^2+b^2}$.

In practical situations, because of the existence of the geometric lens distortion, the projection point $I(u,v)$ in the image plane might be shifted erroneously. So, the real position of the point I in the image coordinate system should be calibrated by proper geometric correction for accurate image unwarping even in the SVP case. Some techniques for this purpose can be found in [6,7] and are followed in this study. The details are omitted.

On the other hand, to estimate the intrinsic parameters of a paracatadioptric omni-camera system, a calibration procedure should be performed before unwarping omni-images into perspective-view ones. In [8,9], using a single view of three lines, Geyer et al. derived analytic calibration solutions for the focal length, the image center, and the aspect ratio of a paracatadioptric camera. In [10], Kang

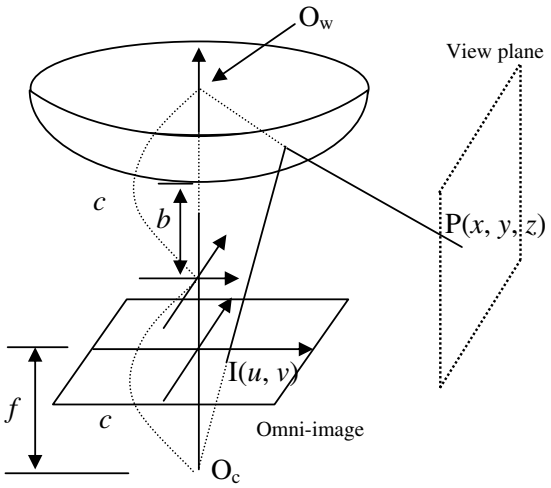

Fig. 1. An SVP hypercatadioptric camera where O_w is the origin of the world coordinate system (also one focus of the hyperbolic curve), and O_c is the optical center (another focus of the hyperbolic curve).

used the consistency condition of pair-wise tracked point features across a sequence of paracatadioptric images to calibrate the same parameters. These approaches basically deal with the calibration problem of an SVP paracatadioptric camera, and misalignment between the mirror and the camera components (including the lens and the CCD sensor) was not considered. That is, the image plane was assumed to be parallel to the base plane of the mirror in these approaches, and only the intrinsic parameters of the cameras were taken into account in the calibration. The quality of the unwarped image is severely degraded when equations derived from a system configuration not meeting such an SVP assumption are used in the unwarping process, even when the intrinsic parameters of the camera have been calibrated.

On the contrary, when a non-SVP camera is used, for example, for the reason to increase the FOV, the system configuration parameters related to the pose of the mirror relative to that of the camera, in addition to the intrinsic camera parameters, need be calibrated. In [11], Aliaga developed a calibration model using a beacon-based pose estimation algorithm for a catadioptric camera which includes a parabolic mirror and a perspective lens. This mirror/lens combination is a non-SVP design, and the adopted camera model, like Tsai's [6], has eleven parameters, five intrinsic and six extrinsic. But the physical meanings of Aliaga's extrinsic parameters are different from those of Tsai's, with the translation vector representing the offset between the center point of the mirror base plane and that of the image plane, and the rotation vector representing the orientation of the mirror base plane with respect to a world space system. Also, the mirror base plane is assumed to be parallel to the image plane. The calibrated data were used to estimate the pose of the camera with respect to the world space system.

A more complete calibration procedure for a catadioptric camera with a parabolic mirror and a perspective lens, which estimates the intrinsic camera parameters and the pose of the mirror relative to the camera, appeared in Fabrizio et al. [12]. The images of two circles on two planes existing in the mirror were used to calibrate the intrinsic camera parameters and the system configuration parameters. But no discussion was made about how to use the calibrated parameters to modify the mapping described by Eqs. (1) to get an accurate unwarped perspective-view image from an omni-image.

3. Proposed method for calibrating camera pose with respect to mirror

In this section, the proposed method for calibrating the camera pose with respect to the mirror of a hypercatadioptric camera system is described. The system configuration and the relationships among the involved coordinate systems are described first, and the proposed calibration process is presented next. The camera pose with respect to the mirror is derived finally, using the calibrated system parameters.

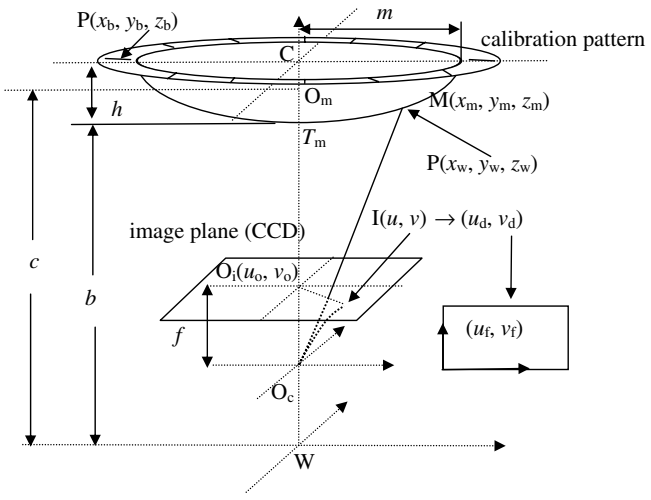

Fig. 2. The configuration of a hypercatadioptric camera used in this study.

3.1. System configuration and coordinate system relationships

The configuration of a hypercatadioptric camera and the related coordinate systems used in this study are depicted in Fig. 2. First, we define a world coordinate system with its origin W taken to be the middle point between the foci of the two arms of the hyperbolic curve defined by the mirror surface. Let b be the distance from W to the tip T_m of the mirror, c the distance from W to a focus O_m of an arm of the hyperbolic curve, h the height of the mirror (measured at T_m), and m the radius of the circular-shaped mirror base. Then, a point $M(x_m, y_m, z_m)$ on the mirror surface with respect to W can be described by the following equations according to Eq. (2):

$$z_m = b\sqrt{1+\frac{r_m^2}{a^2}}, \quad r_m^2 = x_m^2 + y_m^2, \tag{3}$$

where $a = \sqrt{c^2 - b^2}$. The optical center O_c of the camera lens is taken to be the origin of the 3D camera coordinate system, and the optical axis of the camera is assumed to align with the z-axis of the world coordinate system. Accordingly, the center $O_i(u_0, v_0)$ of the 2D image coordinate system, which is the projection point of the optical axis on the image plane described by $z = f$, is $(0,0)$. The mirror parameters a, b, h, and m, and the physical size of the CCD sensor may be obtained from the specifications of the hypercatadioptric camera.

Next, we define a *base coordinate system* on the mirror with its origin taken to be the center C of the bottom circle of the mirror. The base plane of the mirror is located at the plane $z = 0$ of the base coordinate system. A point $P(x_b, y_b, z_b)$ on the ring-shaped calibration pattern on the base plane with respect to the origin of the camera coordinate system can be expressed as follows:

$$[x\ y\ z]^T = R[x_b\ y_b\ z_b]^T + T, \tag{4}$$

where R is a 3×3 rotation matrix with three rotation angles ϕ (pitch), θ (yaw), and ψ (tilt) around the x-, y-, and z-axes of the base coordinate system, respectively, and T is a translation vector described by $T=[T_x\ T_y\ T_z]^{\mathrm{T}}$. Eq. (4) respresents a relationship from the base coordinte system to the camera coordinate system. We will transform the relationship into one from the camera coordinate system to the base coordinte system in Section 3.3, which represents the pose of the camera with respect to the mirror.

On the other hand, the location of the projection point $\mathrm{I}(u,v)$ in the image plane of a point $\mathrm{P}(x,y,z)$ in the camera coordinate system can be described as follows:

$$u=f\frac{x}{z},\quad v=f\frac{y}{z}. \tag{5}$$

To correct possible geometric distortion of the lens in the radial direction, the following distortion model [6] is adopted in this study:

$$u_{\mathrm{d}}=u+D_x,\quad v_{\mathrm{d}}=v+D_y,$$

where u_{d} and v_{d} are the shifted versions of u and v in the image coordinate system, and D_x and D_y are the amounts of distortion estimated, according to [6], by

$$D_x=\kappa u_{\mathrm{d}}r^2,\quad D_y=\kappa v_{\mathrm{d}}r^2$$

with $r^2=u_{\mathrm{d}}^2+v_{\mathrm{d}}^2$ and κ being the *radial distortion factor* of the lens. Combining the above equations, we get the following equations:

$$u=(1-\kappa r^2)u_{\mathrm{d}},\quad v=(1-\kappa r^2)v_{\mathrm{d}}. \tag{6}$$

In the sequel, (u,v) will be called *ideal image coordinates*, and $(u_{\mathrm{d}},v_{\mathrm{d}})$ *distorted image coordinates*. Finally, since the unit of the image coordinates $(u_{\mathrm{f}},v_{\mathrm{f}})$ used in the computer, called *computer image coordinates* hereafter, is ''pixel'' for discrete images kept in the computer, additional relations between the distorted image coordinates $(u_{\mathrm{d}},v_{\mathrm{d}})$ and the computer image coordinates $(u_{\mathrm{f}},v_{\mathrm{f}})$ must be specified, which may be described by:

$$u_{\mathrm{f}}=S_xu_{\mathrm{d}}+C_x,\quad v_{\mathrm{f}}=S_yv_{\mathrm{d}}+C_y, \tag{7}$$

where S_x and S_y are the *coordinate scaling factors* for the x and y directions, respectively, and (C_x,C_y) are the coordinates of the *origin* of the computer image coordinate system. Here, S_x and S_y, and (C_x,C_y) are some parameters related to the physical properties of the CCD sensors and the computer memory, respectively.

3.2. Proposed calibration process for estimating pose parameters with respect to camera

As mentioned previously, we draw a calibration pattern on a paper ring and attach the ring on the mirror mount around the mirror border for use in the subsequent calibration process. The shape of the calibration pattern consists of an inner circle with a diameter equal to that of the mirror, as well as 16 black marks of short line segments evenly distributed around the circle border. Each short line segment has an end point on the inner circle of the ring, which we call a *calibration point*. The configuration is shown in Fig. 3. An image of this calibration pattern is shown in Fig. 4. It is noted that only 12 marks are visible in the FOV of the camera.

The proposed calibration process in this study includes the following major steps.

(1) *Acquisition of calibration pattern images* At the beginning of the calibration process, an image of the calibration pattern is taken. An example of calibration pattern images is shown in Fig. 4.
(2) *Identification of calibration points* The calibration points on the base plane of the calibration pattern are then identified in the image. Let the coordinates of their projection points in the computer image coordinate system be denoted as $(u_{\mathrm{f}i},v_{\mathrm{f}i})$, $i=0,1,\ldots,n$. On the other hand, the base coordinates $(x_{\mathrm{b}i},y_{\mathrm{b}i},z_{\mathrm{b}i})$ of the calibration points are known in advance, with all the values of $z_{\mathrm{b}i}$ being equal to zeros because the points are located on the base plane.

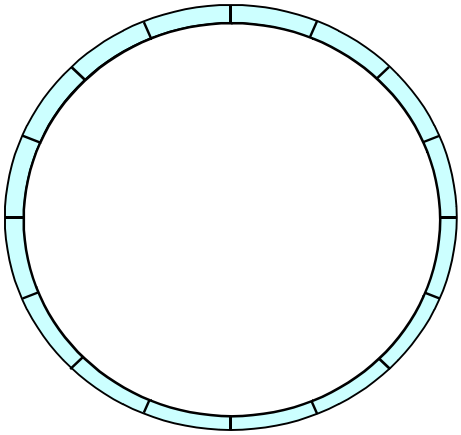

Fig. 3. The calibration pattern designed for use in this study.

Fig. 4. An omni-image of the calibration pattern.

(3) *Computation of physical parameters* Let the image size in the computer image coordinate system be $w_i \times h_i$ and the CCD sensor size be $w_s \times h_s$. Then the parameters S_x, S_y and (C_x, C_y) in Eqs. (7) are calculated in this study in the following way:

$$S_x = \frac{w_i}{w_s}, \quad S_y = \frac{h_i}{h_s}, \quad C_x = \frac{w_i}{2}, \quad C_y = \frac{h_i}{2}.$$

(4) *Computation of intrinsic and extrinsic parameters* The extrinsic parameters R and T in Eq. (4), the intrinsic parameters f in Eqs. (5), and the radial distortion factor κ in Eqs. (6) should be estimated by a certain calibration method. This is accomplished in this study according to the method proposed in [6]. The steps are sketched here. First, from Eqs. (7) we get the distorted image coordinates (u_{di}, v_{di}) of a calibration point in the computer image coordinate system as follows:

$$u_{di} = \frac{u_{fi} - C_x}{S_x}, \quad v_{di} = \frac{v_{fi} - C_y}{S_y}, \tag{8}$$

where (u_{fi}, v_{fi}) are the corresponding computer image coordinates. Next, we combine Eqs. (4)–(8) to derive the following equations:

$$u_{di}(1 + \kappa r_i^2) = \frac{(r_{11}x_{bi} + r_{12}y_{bi} + r_{13}z_{bi} + T_x)f}{r_{31}x_{bi} + r_{32}y_{bi} + r_{33}z_{bi} + T_z},$$
$$v_{di}(1 + \kappa r_i^2) = \frac{(r_{21}x_{bi} + r_{22}y_{bi} + r_{23}z_{bi} + T_y)f}{r_{31}x_{bi} + r_{32}y_{bi} + r_{33}z_{bi} + T_z}, \tag{9}$$

where $r_i^2 = u_{di}^2 + v_{di}^2$. With sufficient known pairs of (u_{di}, v_{di}) and (x_{bi}, y_{bi}, z_{bi}), $i = 0, 1, \ldots, n$, we can solve R, T, κ from Eqs. (9) by Tsai's single view coplanar calibration method [6]. The parameter f is assumed available from the camera specifications.

Fig. 5 shows a calibration result of the pose of the base plane with respect to the camera, which includes the values $(-2.99, 0.96, 88.67)$ of the translation vector T in the unit of mm and the values $(0.013, 0.035, 0.007)$ of the three rotation angles ϕ, θ, and ψ of the rotation matrix R in the unit of radian. The real coordinates of the 12 calibration points are described by the square-bracketed coordinates $[x_i, y_i]$ in Fig. 5. After calibration, the detected image coordinates of the calibration points are back-projected onto the base plane, and the results are described by the angle-bracketed coordinates $\langle x_i, y_i \rangle$, which are also shown in Fig. 5.

3.3. Proposed calibration process for deriving pose parameters with respect to mirror

The pose of the base plane with respect to the camera is composed of the rotation matrix R and the translation vector T derived above. To obtain the pose of the camera with respect to the mirror, we have to transform Eq. (4) into a form similar to those specified in Eqs. (1). The origin of the mirror coordinate system is defined at one focus of the hyperbolic mirror surface (denoted by O_m in Fig. 2). The mirror plane $z = 0$ is taken to be parallel to the base plane at a distance of $d = (b + h) - c$. The z-axis of the mirror coordinate system is aligned with the z-axis of the base coordinate system.

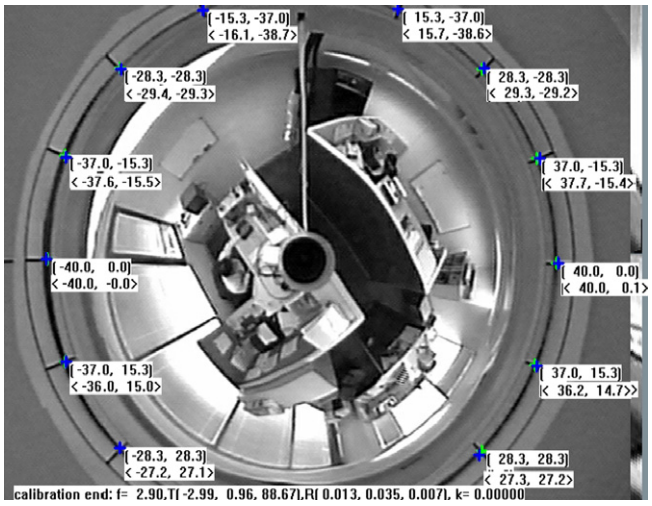

Fig. 5. The calibration result of a hypercataoptric camera used in this study.

It is known that R has the rotation angles (ϕ, θ, ψ) with respect to the x-, y-, and z-axes respectively, and T has the values (T_x, T_y, T_z). To map a point (x, y, z) in the camera coordinate system into a point (x_b, y_b, z_b) in the base coordinate system, the following equation may be applied:

$$\begin{bmatrix} x_b \\ y_b \\ z_b \end{bmatrix} = \begin{bmatrix} r'_{11} & r'_{12} & r'_{13} \\ r'_{21} & r'_{22} & r'_{23} \\ r'_{31} & r'_{32} & r'_{33} \end{bmatrix} \begin{bmatrix} x \\ y \\ z \end{bmatrix} - \begin{bmatrix} T_x \\ T_y \\ T_z \end{bmatrix},$$

where the new rotation matrix

$$R' = \begin{bmatrix} r'_{11} & r'_{12} & r'_{13} \\ r'_{21} & r'_{22} & r'_{23} \\ r'_{31} & r'_{32} & r'_{33} \end{bmatrix}$$

is obtained by reversing the signs of (ϕ, θ, ψ) in Eq. (4).

Because the base plane and the mirror plane are apart with a distance of d, the coordinates (x_b, y_b, z_b) of a point in the base coordinate system with origin C are related to the coordinates (x_w, y_w, z_w) of a point in the mirror coordinate system with origin O_m by the following equalities:

$$\begin{aligned} x_w &= x_b = xr'_{11} + yr'_{12} + zr'_{13} - T_x, \\ y_w &= y_b = xr'_{21} + yr'_{22} + zr'_{23} - T_y, \\ z_w &= z_b + d = xr'_{31} + yr'_{32} + zr'_{33} - T_z + (b + h) - c. \end{aligned} \tag{10}$$

So, the position (x_{cw}, y_{cw}, z_{cw}) of the camera origin O_c in the mirror coordinate system may be derived from that of the mirror origin O_m by setting (x, y, z) in Eqs. (10) to be $(0, 0, 0)$:

$$x_{cw} = -T_x, \quad y_{cw} = -T_y, \quad z_{cw} = -T_z + (b + h) - c. \tag{11}$$

Finally, given the coordinates (u,v,f) of a point I in the camera coordinate system where (u,v) is the ideal image coordinates of I, the corresponding coordinates (x_i,y_i,z_i) of I in the mirror coordinate system, according to Eqs. (10), may be derived to be:

$$\begin{aligned} x_i &= ur'_{11} + vr'_{12} + fr'_{13} - T_x, \\ y_i &= ur'_{21} + vr'_{22} + fr'_{23} - T_y, \\ z_i &= ur'_{31} + vr'_{32} + fr'_{33} - T_z + (b+h) - c. \end{aligned} \tag{12}$$

4. Back-projection of image point

As a summary of the discussions in Section 3, we redraw the camera model as shown in Fig. 6 from the viewpoint of image projection. In Fig. 6, the angles of pitch ϕ_c, yaw θ_c, and tilt ψ_c are respectively the negative values of the calibrated rotation angles in Eq. (4). When the pose of the camera with respect to the mirror is determined in a way as described in Section 3.3, a point $I(u,v)$ in the image plane can uniquely determine a reflective ray R_r from the mirror surface and so a corresponding mirror surface point $M(x_m,y_m,z_m)$. In turn, at point M there will be an incident ray R_i corresponding to R_r with its incident orientation being determined by the mirror surface geometry. Let the direction of R_i be specified by a unit vector denoted by $\vec{w}_u = [w_x w_y w_z]^T$. In this section, we will derive a set of equations to specify a mapping F from the coordinates (u,v) of point I to the elements (w_x,w_y,w_z) of the unit vector $\vec{w}_u$. To be simple, we denote this mapping as $\vec{w}_u = F(I)$. This mapping is constrained, according to the optical reflection principle, by the following two rules.

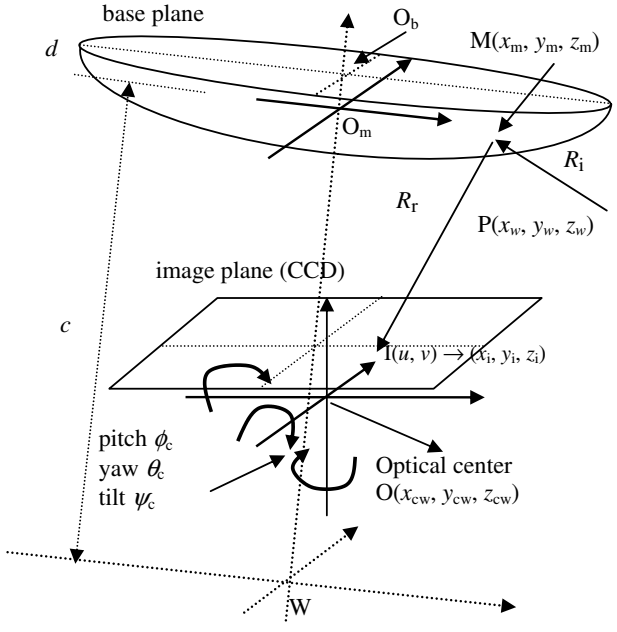

Fig. 6. The image projection model where O_m is the origin of the mirror coordinate system, and O_b is the origin of the base coordinate system.

(1) *Co-planarity constraint*: the unit normal $\vec{n}$ of the mirror surface at point M and the two rays, R_i and R_r, are co-planar.
(2) *Reflection constraint*: the *incident angle* of R_i is equal to the *reflection angle* of R_r.

In the sequel, all the derived formulas are based on the mirror coordinate system.

4.1. Derivation of unit normal vector $\vec{n}$

Fig. 7 depicts the unit normal vector $\vec{n}$ at point $M(x_m,y_m,z_m)$ on a plane passing through the z-axis of the mirror coordinate system with the tilt angle φ, denoted as P_n. The vector $\vec{n}$ can be decomposed into two orthogonal vectors $\vec{n}_m$ and $\vec{n}_z$, where the vector $\vec{n}_m$ is on a plane P_M perpendicular to P_n located at $z = z_m$ and $\vec{n}_z$ is parallel to the z-axis of the mirror coordinate system. The tilt angle by definition is equal to

$$\varphi = \tan^{-1}\frac{y_m}{x_m}. \tag{13}$$

On the other hand, we want to derive the equation of the mirror surface in the mirror coordinate system. Eqs. (3) describes the mirror surface in the world coordinate system. So, a shift $-c$ should be added to the z-value in Eqs. (3), resulting in

$$z_m = -c + b\sqrt{1 + \frac{r_m^2}{a^2}}, \quad r_m^2 = x_m^2 + y_m^2, \tag{14}$$

where r_m may be regarded as a polar coordinate composed of the coordinates of x_m and y_m.

Because the mirror surface is rotationally symmetric in the x- and y-directions, we can consider the *polar coordinates* (r_m,z_m) only, i.e., point M may be thought to be

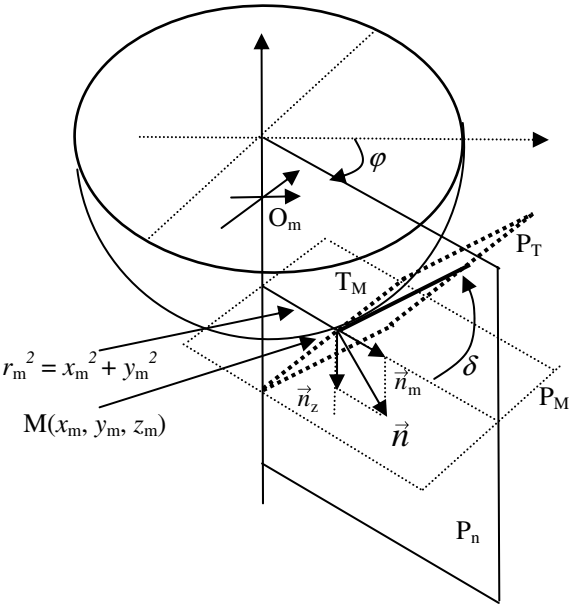

Fig. 7. The unit normal vector $\vec{n}$.

located at (r_m, z_m). Also, let the tangent plane at point M perpendicular to $\vec{n}$ be denoted as P_T, and let the intersection line of P_T and P_n be denoted as T_M. Now, the value of the angle δ of T_M with respect to the plane P_M at point M with polar coordinates (r_m, z_m) on the mirror surface may be derived, by taking the inverse tangent value of a partial derivative of z_m in (14) with respect to r_m, to be

$$\delta = \tan^{-1}\frac{\partial z_m}{\partial r_m} = \tan^{-1}\frac{br_m}{a\sqrt{r_m^2+a^2}} = \tan^{-1}\frac{b^2 r_m}{a^2 z_m}. \quad (15)$$

Accordingly, we can derive the values $\sin\delta$ and $\cos\delta$ as follows:

$$\sin\delta = \frac{br_m}{\sqrt{a^4+c^2r_m^2}}, \cos\delta = \frac{a\sqrt{a^2+r_m^2}}{\sqrt{a^4+c^2r_m^2}}. \quad (16)$$

Finally, it is not difficult to derive the unit normal vector at point $M(x_m, y_m, z_m)$ to be $\vec{n} = [\sin\delta\cos\varphi \sin\delta\sin\varphi - \cos\delta]^T$ according to the geometry shown in Fig. 7.

4.2. Use of co-planarity constraint

The co-planarity constraint on the unit normal $\vec{n}$ of the mirror surface at point M and the two rays, R_i and R_r, is shown in Fig. 8, and can be described by the following equality according to vector analysis:

$$(\vec{o}\times\vec{n})\cdot\vec{w} = 0,$$

or equivalently,

$$\begin{bmatrix} i & j & k \\ (x_{cw}-x_m) & (y_{cw}-y_m) & (z_{cw}-z_m) \\ \sin\delta\cos\varphi & \sin\delta\sin\varphi & -\cos\delta \end{bmatrix}\begin{bmatrix}(x_w-x_m)\\(y_w-y_m)\\(z_w-z_m)\end{bmatrix} = 0,$$

where "×" and "·" denote the cross and inner product operators for vectors, respectively; $\vec{w} = [(x_w-x_m)\ (y_w-y_m)\ (z_w-z_m)]^T$ specifies the direction of the incident ray R_i; $[i\ j\ k]^T$ is a unit vector; and $\vec{o} = [(x_{cw}-x_m)(y_{cw}-y_m)\ (z_{cw}-z_m)]^T$ specifies the direction of the reflection ray R_r. By computing the above matrix product and substituting the result with the following notations

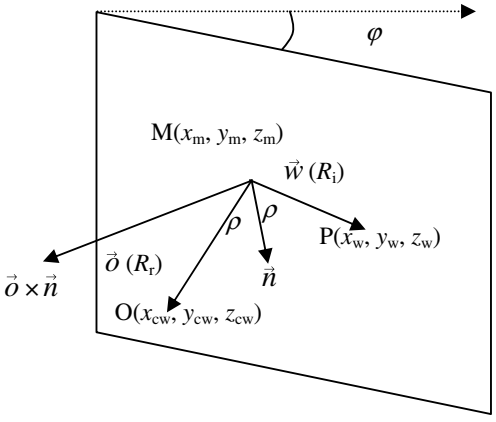

Fig. 8. The co-planar vectors and the cross product.

$$K_{m1} = (y_m - y_{cw})\cos\delta + (z_m - z_{cw})\sin\delta\sin\varphi,$$
$$K_{m2} = (x_m - x_{cw})\cos\delta + (z_m - z_{cw})\sin\delta\cos\varphi,$$
$$K_{m3} = (x_{cw} - x_m)\sin\delta\sin\varphi - (y_{cw} - y_m)\sin\delta\cos\varphi,$$
$$x_n = (x_w - x_m),\quad y_n = (y_w - y_m),\quad z_n = (z_w - z_m),$$

we get

$$K_{m1}x_n - K_{m2}y_n + K_{m3}z_n = 0. \quad (17)$$

4.3. Use of reflection constraint

The aforementioned reflection constraint, which indicates the identicalness of the incident angle to the reflection angle, may be expressed by the following equalities:

$$\frac{\vec{w}\cdot\vec{n}}{\|\vec{w}\|\|\vec{n}\|} = \cos\rho, \quad \cos\rho = \frac{\vec{o}\cdot\vec{n}}{\|\vec{o}\|\|\vec{n}\|}, \quad (18)$$

where ρ denotes the two identical angles. The second equality in Eqs. (18) may be expanded to be

$$\cos\rho = \frac{(x_{cw}-x_m)\sin\delta\cos\varphi + (y_{cw}-y_m)\sin\delta\sin\varphi - (z_{cw}-z_m)\cos\delta}{\sqrt{(x_{cw}-x_m)^2+(y_{cw}-y_m)^2+(z_{cw}-z_m)^2}}. \quad (19)$$

On the other hand, the three components of the unit vector $\vec{w}_u = \frac{\vec{w}}{\|\vec{w}\|} = [w_x w_y w_z]^T$, by definition, can be calculated as follows:

$$w_x = \frac{x_n}{\sqrt{x_n^2+y_n^2+z_n^2}}, \quad w_y = \frac{y_n}{\sqrt{x_n^2+y_n^2+z_n^2}},$$
$$w_z = \frac{z_n}{\sqrt{x_n^2+y_n^2+z_n^2}}.$$

Then, the first equality in Eqs. (18) can be derived to be as follows:

$$\begin{aligned}\frac{\vec{w}\cdot\vec{n}}{\|\vec{w}\|\|\vec{n}\|} &= \vec{w}_u\cdot\vec{n},\\ &= [w_x w_y w_z]^T\cdot[\sin\delta\cos\varphi\ \ \sin\delta\sin\varphi\ \ -\cos\delta]^T,\\ &= w_x\sin\delta\cos\varphi + w_y\sin\delta\sin\varphi - w_z\cos\delta,\\ &= \cos\rho, \end{aligned} \quad (20)$$

where $\cos\rho$ can be computed by Eq. (19) above.

4.4. Calculating direction of incident ray

If the values (x_n, y_n, z_n) are not equal to $(0,0,0)$, Eq. (17) may be rewritten as

$$K_{m1}\frac{x_n}{\sqrt{x_n^2+y_n^2+z_n^2}} - K_{m2}\frac{y_n}{\sqrt{x_n^2+y_n^2+z_n^2}} + K_{m3}\frac{z_n}{\sqrt{x_n^2+y_n^2+z_n^2}} = 0,$$

which is equivalent to

$$K_{m1}w_x - K_{m2}w_y + K_{m3}w_z = 0. \quad (21)$$

On another hand, the norm of the unit vector $\vec{w}_u$ is equal to 1, i.e.,

$$w_x^2 + w_y^2 + w_z^2 = 1. \quad (22)$$

Using Eqs. (20)–(22), we can solve the three unknown parameters w_x, w_y, and w_z in the following way.

First, we eliminate the unknown w_z in Eqs. (20) and (21) to get

$$w_y = A_m w_x + B_m, \tag{23}$$

where

$$A_m = \frac{K_{m1}\cos\delta + K_{m3}\sin\delta\cos\varphi}{K_{m2}\cos\delta - K_{m3}\sin\delta\sin\varphi},$$
$$B_m = \frac{-K_{m3}\cos\rho}{K_{m2}\cos\delta - K_{m3}\sin\delta\sin\varphi}.$$

Next, we eliminate the unknown w_y in Eqs. (20) and (21) to get

$$w_z = C_m w_x + D_m, \tag{24}$$

where

$$C_m = \frac{(K_m\sin\varphi + K_{m2}\cos\varphi)\sin\delta}{K_{m2}\cos\delta - K_{m3}\sin\delta\sin\varphi},$$
$$D_m = \frac{-K_{m2}\cos\rho}{K_{m2}\cos\delta - K_{m3}\sin\delta\sin\varphi}.$$

Finally, substituting Eqs. (23) and (24) into Eq. (22) and reducing the result, we get

$$w_x = \frac{-(A_m B_m + C_m D_m) \pm \sqrt{(A_m B_m + C_m D_m)^2 - (1 + A_m^2 + C_m^2)(B_m^2 + D_m^2 - 1)}}{(1 + A_m^2 + C_m^2)}. \tag{25}$$

There are two possible solutions for w_x, and using the relationship between the coordinates (x_i, y_i, z_i) of the image point and the coordinates (x_{cw}, y_{cw}, z_{cw}) of the optical center, all in the mirror coordinate system, we can determine one of them as the correct solution. The details are omitted here. After w_x is obtained, w_y and w_z can be computed accordingly by Eqs. (23) and (24).

4.5. Calculating coordinates of mirror surface point in terms of image point coordinates

In Sections 4.1–4.4, we have derived the elements (w_x, w_y, w_z) of the unit vector $\vec{w}_u$ in terms of the coordinates (x_m, y_m, z_m) of the mirror surface point M. Here, we further want to derive (x_m, y_m, z_m) in terms of the coordinates (u, v) of the image point I to complete the derivations of the formulas for specifying the mapping $\vec{w}_u = F(I)$. The coordinates (u, v) can be calculated from a point (u_f, v_f) in the computer image coordinate system by Eqs. (8) and (6). Also, the coordinates (x_i, y_i, z_i) of the image point I in the mirror coordinate system can be calculated from Eqs. (12) which are repeated in the following:

$$x_i = ur'_{11} + vr'_{12} + fr'_{13} - T_x,$$
$$y_i = ur'_{21} + vr'_{22} + fr'_{23} - T_y,$$
$$z_i = ur'_{31} + vr'_{32} + fr'_{33} - T_z + (b + h) - c.$$

Now, referring to Fig. 8, we see that both the tilt angle of the point I and that of its back-projection point M on the mirror surface relative to the camera coordinate system are equal. Let both angles be denoted by ϕ. Then, it is easy to see from the geometry in the figure that

$$\tan\phi = \frac{y_i - y_{cw}}{x_i - x_{cw}} = \frac{y_m - y_{cw}}{x_m - x_{cw}},$$

or equivalently, that

$$y_m = y_{cw} - x_{cw}\tan\phi + x_m\tan\phi. \tag{26}$$

Combining Eqs. (12) and (26) and using the following notations

$$K_1 = y_{cw} - x_{cw}\tan\phi,$$
$$K_2 = \frac{(z_i - z_{cw})}{x_i - x_{cw}},$$
$$K_3 = z_{cw} + c - x_{cw}K_2,$$
$$K_4 = b^2(1 + \tan^2\phi) - a^2K_2^2,$$
$$K_5 = b^2K_1\tan\phi - a^2K_2K_3,$$
$$K_6 = a^2b^2 + b^2K_1^2 - a^2K_3^2,$$

we get, after some derivations and reductions, the following result for x_m:

$$x_m = \frac{-K_5 \pm \sqrt{K_5^2 - K_4K_6}}{K_4}. \tag{27}$$

There are two possible solutions for x_m in the above equation, and we can get the correct one by checking the condition that x_m and x_i are at the same side with respect to x_{cw}, or equivalently, that the value of the product $(x_m - x_{cw})(x_i - x_{cw})$ is larger than or equal to zero. Also, using Eq. (26), we can get y_m. And finally the value of z_m can be calculated from Eqs. (14) which are repeated as follows:

$$z_m = -c + b\sqrt{1 + \frac{r_m^2}{a^2}}, r_m^2 = x_m^2 + y_m^2. \tag{28}$$

5. Experimental results

We show in this section the experimental results of two unwarping cases with two different omni-images as inputs, one being a pseudo-image and the other a real image taken by our hypercatadioptric camera.

5.1. Unwarping of a pseudo-image into perspective views

We first describe how we create the pseudo-image for the first unwarping experiment. For this purpose, we used the calibration data obtained in Section 3, which include the translation parameters $(-2.99, 0.96, 88.67)$ (in the unit of mm); the rotation angles $(0.013, 0.035, 0.007)$ (in the unit of radian); the radial distortion factor $\kappa = 0.0$; and the focal length $f = 2.9$ mm. Then, we used the mapping equations obtained in Section 4 to warp a pseudo target as shown in Fig. 9 into the image plane to get the desired pseudo omni-image as shown in Fig. 10. The procedure

was mentioned in Section 5.2, and the details are described in the following.

The pseudo target includes two parts, namely, a ground region with the area of $20 \times 20\ m^2$ and consisting of 400 grids with each being of the size of $1 \times 1\ m^2$, as well as an L-shaped wall with the height of 1.0 m and a side width of 2.8 m. The L-shaped wall is placed near the center of the ground region. In simulating the image taking work, the target was laid under our hypercatadioptric camera and the normal vector of the ground region at the region center aligns with the z-axis of the mirror coordinate system. The distance of the region center from the origin of the mirror coordinate system is 2 m. The resulting pseudo-image of Fig. 10 is of the size of 640×480 pixels.

We then describe how we unwarped the pseudo-image into perspective-view images. We selected two perspective-view planes, one being from a side view and the other from the top view. As shown in Fig. 11, each perspective-view plane is a rectangular region, which was used to capture the rays back-projected from the image plane. Each rectangular region was divided into 320×240 units representing a 320×240 image.

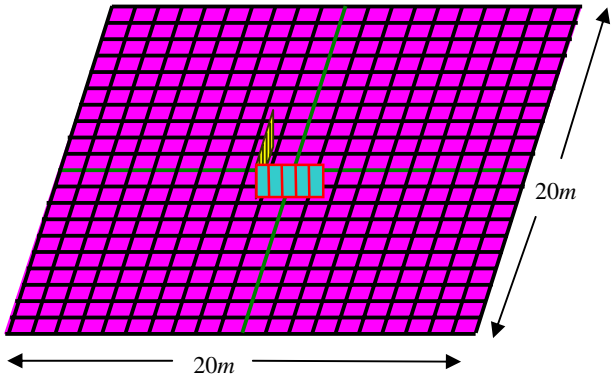

Fig. 9. A pseudo target of size 20×20 m with an L-shaped wall at the center position.

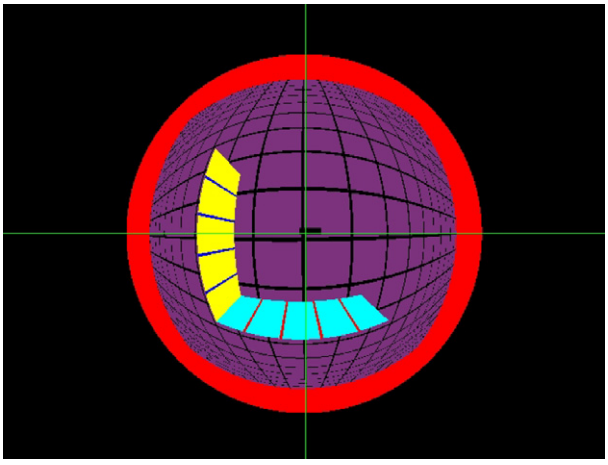

Fig. 10. The warped image of the pseudo target in Fig. 9.

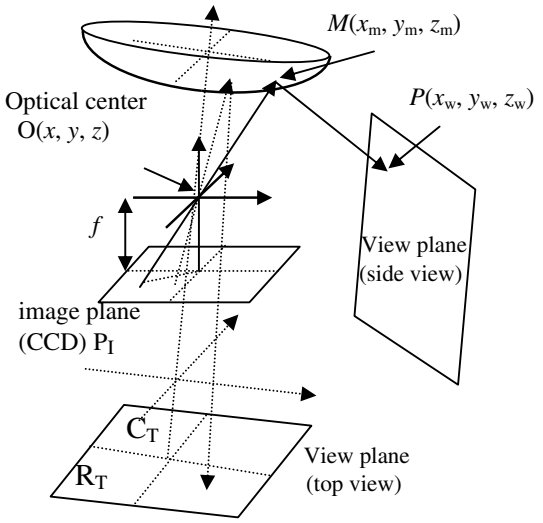

Fig. 11. View planes defined in the real world for unwarped images.

The top-view region R_T is $4 \times 4\ m^2$ in size, parallel to the x–y plane of the mirror coordinate system. The normal vector of R_T at the center C_T of R_T aligns with the z-axis of the mirror coordinate system, and C_T is 2 m below the origin of the mirror coordinate system. Fig. 12(a–c) are the unwarping results in R_T with different calibration parameter settings. Here, Fig. 12(a) was produced using the same translation and rotation parameters as those used in yielding Fig. 10. In Fig. 12(b), the three rotation angles were all set to be zero. And in Fig. 12(c), we further set the two translation parameters T_x and T_y to be zero (meaning perfect alignment of the camera with respect to the mirror). We can see in Fig. 12(a) that our derived equations can be used to unwarp the pseudo-image of Fig. 10 perfectly within the top-view region R_T. Fig. 12(b) and (c) tell us that insufficient calibration of the hypercatadioptric camera will produce distorted unwarping results.

On the other hand, we show some results coming from inappropriate unwarping of the input pseudo-image Fig. 10 using Eqs. (1) under the erroneous assumption that the camera is an SVP system. They are shown in Fig. 12(d–f), which are the results coming from the uses of three different CCD sensors of sizes 3.2×2.4, 1.6×1.2, and $0.8 \times 0.6\ mm^2$, respectively. The actual size of our CCD camera sensor is the first one, namely, $3.2 \times 2.4\ mm^2$ and the corresponding unwarping result is the image shown in Fig. 12(d). But the visible scope of the image region in the figure is too small to show the entire unwarping result. For the reason of comparison, we therefore assume the other two sensor sizes for our camera to yield Fig. 12(e) and (f) for the purpose of showing the unwarping results more clearly. Note that the sensor size settings of Fig. 12(e) and (f) are unreasonable for a real CCD sensor. From Fig. 12(f), it is obviously seen that the result is worse than the perfect one shown in Fig. 12(a).

Fig. 13(a) through (d) show the unwarping results on four perspective-view planes. Each perspective-view plane

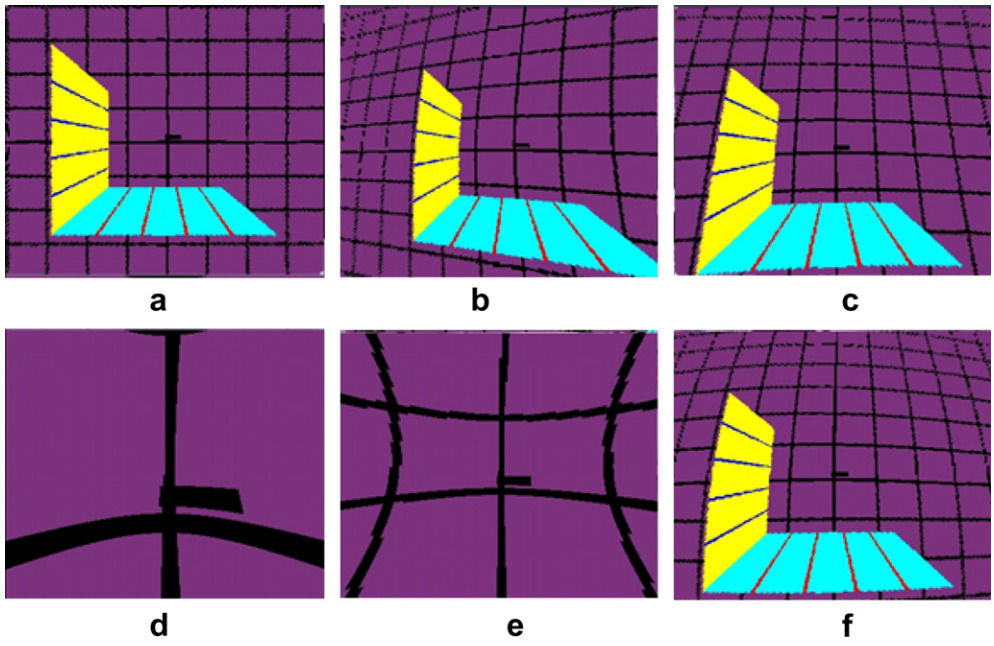

Fig. 12. Unwarped images of Fig. 10 (top view), (a) has the same T(T_x, T_y, T_z) and R(R_x, R_y, R_z) as those for yielding Fig. 10, (b) has the setting $R_x = R_y = R_z = 0$, and (c) has the further setting $T_x = T_y = 0$, (d–f) Results using Eq. (1) with different CCD sensor sizes of 3.2×2.4, 1.6×1.2, and 0.8×0.6, respectively.

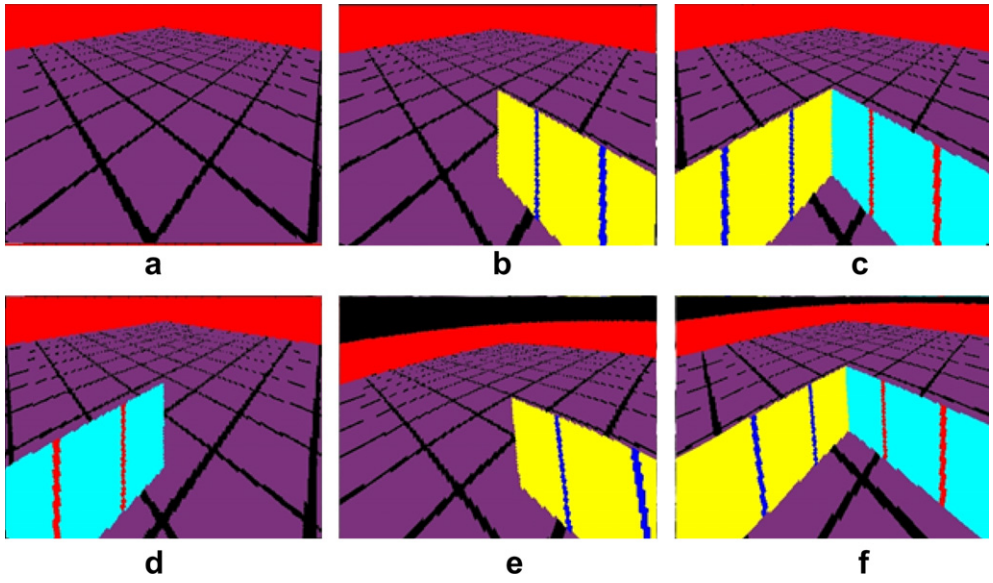

Fig. 13. Unwarped images of Fig. 10 from 4 side views. (a–d) Results using the proposed method with the same T and R as those for yielding Fig. 10. (a–d) Results with different span of view angle, $1.5\pi \sim 2.0\pi$, $1.0\pi \sim 1.5\pi$, $0.5\pi \sim 1.0\pi$, and $0.0\pi \sim 0.5\pi$, respectively. (e) and (f) Results using Eqs. (1) with different spans of viewing angle, as (b) and (c), respectively.

is set parallel to the z-axis of the mirror coordinate system with a view-angle span of 90° in the x–y plane and at a distance of $\sqrt{2}$ m from the z-axis of the mirror coordinate system. The unwarping result is projected into a region in each perspective-view plane with a height of 2 m and a width of $2\sqrt{2}$ m. Fig. 13(a) through (d) are the unwarping results using our derived equations in the four perspective-view planes. The settings of the translation parameters and the rotation angles are the same as those for Fig. 12(a) through (d). Fig. 13(e) and (f) are the unwarping results by Eqs. (1) in the same perspective-view planes as those used for Fig. 13(b) and (c) but under the SVP assumption and with the CCD sensor size of $0.8 \times 0.6\ \text{mm}^2$. Note especially that the vertical lines in Fig. 13(e) and (f) can be seen to be slanted erroneously.

5.2. Unwarping of a real image into perspective views

Figs. 14 and 15 are the unwarping results of a real image shown previously in Fig. 4 taken by our camera. The parameter settings used for computing Figs. 14 and 15 are the same as those used to produce Figs. 12 and 13, except that the pseudo-image is now replaced by the real image. Or more specifically, Fig. 14(a) through (f) correspond to Fig. 12(a) through (f), respectively, and Fig. 15(a) through (f) to Fig. 13(a) through (f), respectively. Comparing Fig. 14(a) with (f), and Fig. 15(b) and (c) with Fig. 15(e) and (f), respectively, we can see that the unwarping results obtained by our methods are better than those obtained under the SVP assumption. Especially, the vertical lines in Fig. 15(e) and (f) as well can be seen to be slanted. Such situations are not seen in our results in Fig. 15(b) and (c).

It is noted that the images of the above-mentioned experiments were obtained using some methods proposed

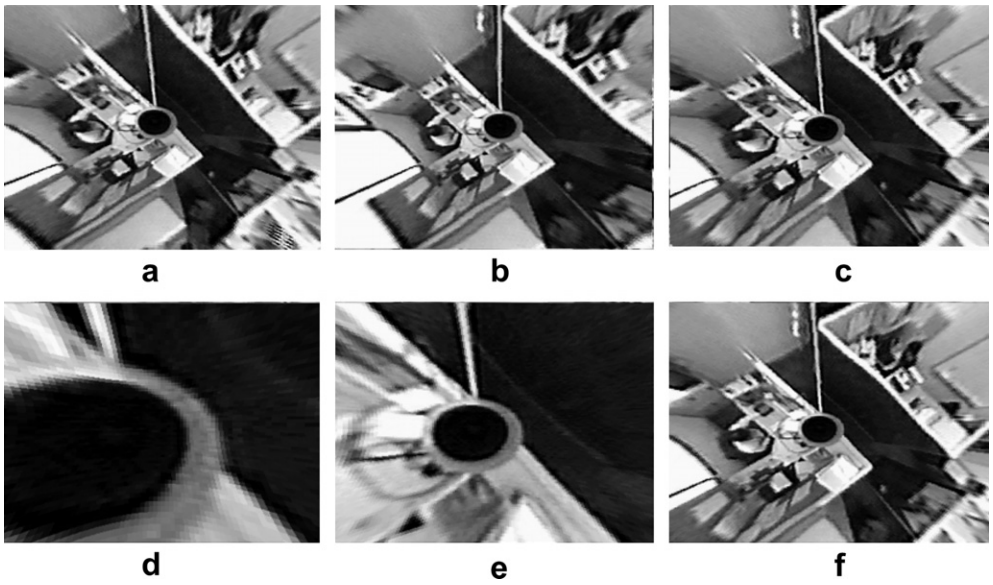

Fig. 14. Unwarped images of a real scene in Fig. 4 (top view), (a) has the T(T_x, T_y, T_z) and R(R_x, R_y, R_z) mentioned in Section 3.2 after calibration, (b) has the setting $R_x = R_y = R_z = 0$, and (c) has the further setting $T_x = T_y = 0$. (d–f) Results using Eq. (1) with different CCD sensor size of 3.2×2.4, 1.6×1.2, and 0.8×0.6 mm^2, respectively.

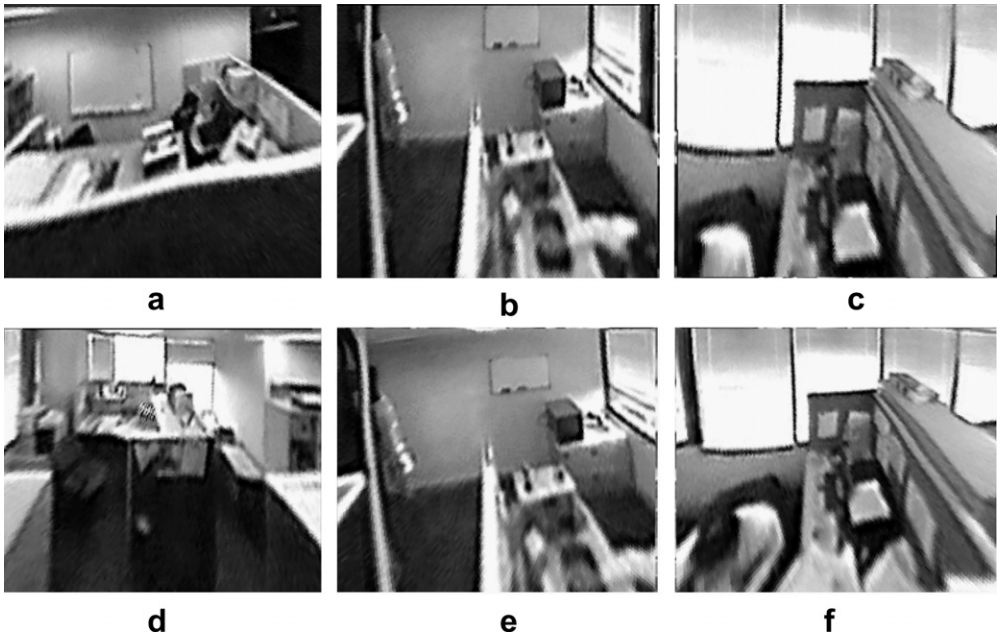

Fig. 15. Unwarped images of a real scene in Fig. 4 (Side view). (a–d) Results using the proposed method with the same T and R as those for yielding Fig. 2.14. (a–d) Results with different span of view angle, $1.5\pi \sim 2.0\pi$, $1.0\pi \sim 1.5\pi$, $0.5\pi \sim 1.0\pi$, and $0.0\pi \sim 0.5\pi$, respectively. (e) and (f) Results using Eqs. (1) with different span of viewing angle as (b) and (c), respectively.

in our previous paper [13], and the details are omitted here.

6. Conclusions

An approach to systematic calibration and analytic image unwarping for omni-directional non-SVP hypercatadioptric cameras with hyperbolic-shaped mirrors has been proposed. We used the calibrated parameters of the camera to derive precise unwarping equations. The derived equations have been validated to yield the same unwarping results as those yielded by a perfectly designed SVP camera by adjusting the calibrated parameters to fit the SVP constraint. Furthermore, we have shown the advantages of our method over the SVP-constrained method for real cameras by some simulation and experimental results. It is mentioned by the way that the resulting image quality of the unwarped perspective-view image is decided by the structure of the omni-camera, the number of grids placed in the defined perspective-view plane in the world space, as well as the location of the view plane with respect to the omni-camera. Future studies may be directed to enhancing the quality of the images according to the above-mentioned three factors as well as employing the unwarping results for real applications.

Acknowledgement

This work was supported financially by the Ministry of Economic Affairs under Project No. MOEA 93-EC-17-A-02-S1-032 in Technology Development Program for Academia.

References

[1] S.K. Nayar, Catadioptric Omni-directional Camera, in:Proceedings of IEEE Conference on Computer Vision and Pattern Recognition, San-Juan, Puerto Rico, June 1997, pp. 482–488.

[2] S. Baker, S.K. Nayar, A theory of single-viewpoint catadioptric image formation, International Journal of Computer Vision 35 (2) (1999) 175–196.

[3] R. Swaminathan, M.D. Grossberg, S.K. Nayar, Caustics of catadioptric cameras, in: Proceedings of eighth IEEE International Conference on Computer Vision, Vancouver, BC, Canada, vol. 2, July 7–14, 2001, pp. 2–9.

[4] K. Yamazawa, Y. Yagi, M. Yachida, Omni-directional imaging with hyperboloidal projection, in: Proceedings of 1993 IEEE/RSJ International Conference on Intelligent Robots and Systems, Yokohama, Japan, July 26–30, 1993, pp. 1029–1034.

[5] Y. Onoe, N. Yokoya, K. Yamazawa, H. Takemura, Visual surveillance and monitoring system using an omni-directional video camera, in: Proceedings of 14th International Conference on Pattern Recognition, Brisbane, Australia, vol. 1, August 16–20, 1998, pp. 588–592.

[6] R.Y. Tsai, An efficient and accurate camera calibration technique for 3D machine vision, in: Proceedings of IEEE Conference on Computer Vision and Pattern Recognition, Miami Beach, Florida, 1986, pp. 364–374.

[7] J. Salvi, X. Armangué, J. Batle, A comparative review of camera calibrating methods with accuracy evaluation, Pattern Recognition 35 (2002) 1617–1635.

[8] C. Geyer, K. Daniilidis, Paracatadioptric camera calibration, IEEE Transactions on Pattern Analysis and Machine Intelligence 24 (5) (2000) 687–695.

[9] C. Geyer, K. Daniilidis, Catadioptric camera calibration, in: Proceedings of seventh IEEE International Conference on Computer Vision, Corfu, Greece, vol. 1, September 20–25, 1999, pp. 398–404.

[10] S.B. Kang, Catadioptric self-calibration, in: Proceedings of IEEE Conference on Computer Vision and Pattern Recognition, Hilton Head, South Carolina, vol. 1, June 13–15, 2000, pp. 201–207.

[11] D.G. Aliaga, Accurate catadioptric calibration for real-time pose estimation in room-size environments, in: Proceedings of eighth IEEE International Conference on Computer Vision, Vancouver, BC, Canada, vol. 1, July 07–14, 2001, pp. 127–134.

[12] J. Fabrizio, J.P. Tarel, R. Benosman, Calibration of panoramic catadioptric sensors made easier, in: Proceedings of third Workshop on Omni-directional Vision, Copenhagen, Denmark, June 02, 2002, pp. 45–52.

[13] S.W. Jeng, W.H. Tsai, Construction of perspective and panoramic images from omni-images taken from hypercatadioptric cameras for visual surveillance, in: Proceedings of 2004 IEEE International Conference on Networking, Sensing, and Control, Taipei, Taiwan, March 21–23, 2004, pp. 204–209.